Simultaneous measurement of group and phase delay between two photons

D. Branning and A. L. Migdall

Optical Technology Division, NIST, Gaithersburg, Maryland 20899-8441

A. V. Sergienko

Department of Electrical and Computer Engineering, Boston University, Boston, Massachusetts 02215

We report on an experiment to determine both the group and phase delays experienced by orthogonally polarized photon pairs traveling through a birefringent medium. Both types of delay are determined from the same set of coincidence-counting data. The experiment is based on an interference technique using two-photon multipath indistinguishability to produce an interference feature. Earlier work has shown that this interference feature can be used to measure the group velocity of single-photon wave packets in dielectric media. In the current work, the two-photon interferometer has been modified to produce an additional interference feature that is sensitive to the phase velocity of the light. We have used this technique to simultaneously measure the group delay in crystal quartz with a precision of 0.1 fs and the phase delay with a precision of 8 attoseconds. Our analysis clarifies the effects of group and phase delays and shows the unexpected result that dispersive temporal broadening, which is well known to be canceled for the original interferometer setup, is not canceled for this type of ''postponed compensation'' interferometer.

PACS number(s): 42.50.Dv, 42.62.Eh, 07.60.Ly

INTRODUCTION

In the past two decades, the entangled photon pairs spontaneously emitted from parametric down-conversion (PDC) sources have been used for tests of quantum mechanics [1,2], for quantum information processing [3], for metrological applications [4], and for measurement of the differential optical group delays, or polarization-mode dispersion (PMD), in birefringent materials [5,6]. This last application, driven by increasing communication speeds, is becoming more important as the chromatic dispersion of manufactured optical components (particularly communication components such as fibers) is reduced to lower and lower levels. Because type-II phase-matched PDC sources can be arranged to produce pairs of orthogonally polarized but collinearly propagating photons (which can become entangled in their polarizations), it readily lends itself to measurements of differential optical delays. High resolution is possible because the photons of a down-converted pair are created simultaneously, and because the common optical path taken by both photons provides excellent interferometric stability.

Thus far, it has been demonstrated that a common-path version of the Hong-Ou-Mandel (HOM) interferometer [5,7] can be used to make PMD measurements to a precision of ~0.2 fs [6]. The uncertainty of that technique depends on how well one can find the center of an interference feature—the ''dip'' in coincidence count rate seen as a common-path delay is scanned (see Fig. 1). The PMD of a sample is de-termined by measuring the shift in this feature as that sample is inserted into the common path. Here we report on a modification of this configuration that retains this high level of accuracy for the *group* delay, while adding the capability to simultaneously measure the relative *phase* delay between the two photons. The modification consists of relocating the birefringent delay line and the sample from the common path (before the beam splitter) to a ''postponed compensation'' position (after the beam splitter) [8], and then observing the shift in both the dip and the interferometric fringes as the sample is inserted into the post-delay path.

Because the technique is based on HOM interference, we begin with a brief overview of that phenomenon and of the modifications that produce sensitivity to both the group and phase velocity. We then present the results of an experiment demonstrating that the technique can measure group delay in a sample to a precision of 0.1 fs and phase delay to a precision of 8 attoseconds (as). In the Appendix, we present a rigorous derivation of the two-photon interference pattern and its dependence on both the group and phase velocities of the photons in the post-delay material. We also note there that the dispersion cancellation that usually occurs in two-photon interference from cw-pumped PDC sources [9–11] does not occur in this new postponed configuration. This dispersion cancellation is usually one of the main differences between the quantum-interferometric technique and classical methods of determining PMD; the other differences, which
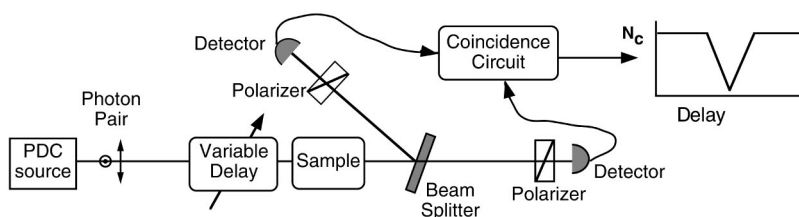

FIG. 1. Generic setup for measuring sample PMD using correlated pairs of orthogonally polarized photons.
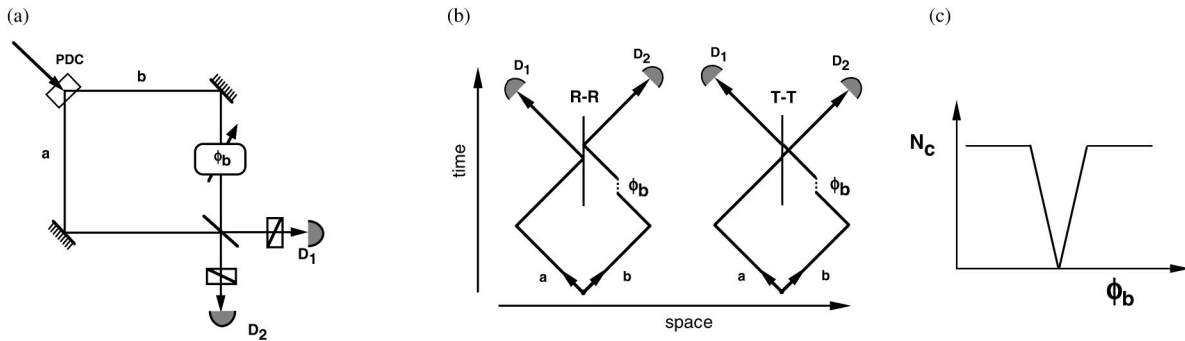
FIG. 2. (a) The HOM interferometer. (b) Feynman-like representations of the two ways to detect a pair of photons in coincidence. (c) The coincidence counting rate as a function of relative delay.

are retained here, are as follows: (i) broadband light may be conveniently produced with a cw source, whose bandwidth may be simply controlled by adjusting the crystal length; (ii) unlike a classical common-path interferometer, differential losses for the two polarizations will not reduce the interference visibility in this coincidence-counting technique; (iii) coincidence counting rejects many sources of background noise and improves interference visibility, while for a classical version the noise could only be somewhat overcome by using bright broadband sources such as ultrashort lasers, as fluorescence scattering would limit their maximum intensities.

HOM INTERFERENCE

In the classic experiment of Hong, Ou, and Mandel [7], two photons from a PDC are brought together at a beam splitter whose output ports are monitored by two photon-counting detectors as in Fig. 2(a).[1] A ''two-photon'' is detected as a coincidence between the two detectors. There are two ways to produce such a coincidence: either both photons are reflected (R-R) or both are transmitted (T-T) by the beam splitter. Because the two-photon amplitudes for double reflection and double transmission are of opposite sign, they can cancel each other completely if a 50/50 beam splitter is used. This cancellation means that the two photons of a pair cannot both be reflected or both be transmitted; thus, they cannot end up at different detectors. If the two detectors are monitored in coincidence, there will be a complete lack of coincidence counts due to this destructive interference.

There is a caveat here: this interference can only occur if the two coincidence pathways, T-T or R-R, cannot be distinguished from one another by any auxiliary measurement, such as the relative arrival time of the photons. The Feynman-like diagrams [Fig. 2(b)] of Pittman et al. [8] show how the coincidence paths become more or less distinguishable as the relative delay (ϕ_b) between the photons is varied. For significantly unequal path lengths (relative to the coherence time of the down-converted light), the R-R and T-T

processes lead to measurably different time separations between the photodetections. This time separation could, in principle, be used to keep track of whether each coincidence event was an R-R or a T-T event. Therefore, these processes are distinguishable and cannot interfere, and the overall coincidence counting rate is then just the sum of the individual rates for each. However, as the path lengths are made more and more equal, the R-R and T-T processes lead to detection time separations that are more and more alike; when the relative delay between the paths is zero, the time separations between the firings of detectors 1 and 2 for the R-R and T-T coincidence events become identical, making these two possible coincidence paths indistinguishable from one another. At this point, the destructive interference of the T-T and R-R amplitudes is complete, and no coincidences will be observed. Thus, as the photon path delay ϕ_b is scanned from a large negative value to a large positive value, the coincidence-counting rate traces out a ''dip'' that can fall to zero at the point of zero path delay [see Fig. 2(c)]. Because this complete destructive interference is in conflict with the predictions of classical optics [1,12], the coincidence dip has become a well-known signature of quantum interference between two photons, or, more precisely, between alternate two-photon paths.

Hong et al. first applied this two-photon interference to measure very short time delays between two photons in air, effectively mapping out the temporal profile of the single-photon wave packet [7]. Later, Steinberg, Kwiat, and Chiao used HOM interference to measure the time delay experienced by single photons in glass [9] or in tunneling through a barrier [13]. They also discovered that the temporal broadening of the photon wave packets that would normally occur due to group-velocity dispersion (GVD) in the glass does not appear in the coincidence-count profile—the GVD is completely canceled because the photons emerging from the parametric down-converter are entangled in frequency.

Several years ago, Pittman and co-authors used a modified HOM interferometer to ask a provocative question: ''Can two-photon interference be considered the interference of two photons?'' Their answer was ''no,'' for their experiment [8] showed that destructive two-photon interference can occur even if the single-photon wave packets do not overlap at the beam splitter, provided that the indistinguishability of the R-R and T-T coincidence events is maintained

---

[1]Note the separated path interferometer diagrams of Figs. 2(a) and 3(a) are, for our purposes, equivalent to the combined path setup of Fig. 1. We use the separated path diagrams here as a conceptual aid.
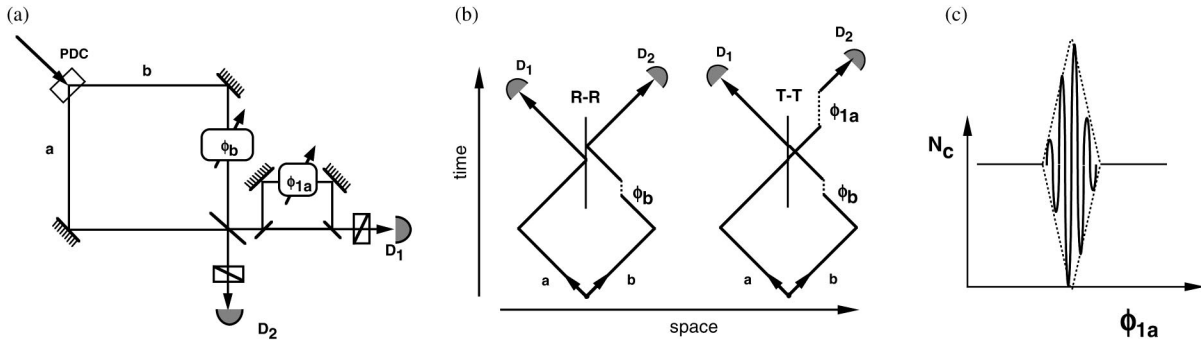
FIG. 3. Postponed-compensation version of the HOM interferometer.

as detected. This was done in their experiment by means of a ''postponed compensation'' delay line, which selectively retards one of the photons *after* the beam splitter in order to equalize the relative time delays for a doubly transmitted or doubly reflected photon pair to reach the detectors [see Fig. 3(a)].

Though it was not important for their demonstration of what does and does not constitute ''two-photon interference,'' another feature of the scheme of Pittman *et al.* is a modulation between a constructive-interference ''peak'' and a destructive-interference ''dip'' in the coincidence rates as the amount of post-delay is varied [see Fig. 3(c)] [14]. With the help of the Feynman-like diagrams of Fig. 3(b), we can see that indistinguishability now occurs for a specific, but nonzero, separation between the detector firing times, and requires a postponed delay that is equal to twice the required delay before the beam splitter. Also note that in the postponed setup there is a delay ϕ_{1a} that occurs in only one of the two coincidence types, while the delay before the beam splitter ϕ_b in both Figs. 2 and 3 is common to both of the coincidence types. It is the fact that in the postponed setup, ϕ_{1a} provides a differential delay between the two coincidence types that allows the fringes of Fig. 3(c) to arise.

In this postponed compensation scheme, the coincidence dip envelope retains its characteristic shape, as determined by the relative group delays between the signal and idler photons. The fringes that arise, however, are sensitive only to the relative *phase* delay acquired at the central frequency of each photon's spectrum.[2] Thus, by monitoring a shift in the position of the envelope and in the position of the underlying fringes as an unknown sample of birefringent material is added to the interferometer, we can simultaneously measure both the group delays and the phase delays imposed on the photons by the sample.

EXPERIMENT

We constructed a common-path HOM interferometer to investigate how precisely the group and phase delays of an unknown sample might be determined. The apparatus, shown in Fig. 4, measures coincidence counting rates as a function of birefringent delay, and produces different results when the delay (and sample) is located either before or after the beam splitter. Our results show how well the system can be used to simultaneously measure both group and phase delays of a sample. To create the photon pairs, a 351.1-nm, 0.5-W Ar$^+$ laser was used to pump a BBO (β-BaB$_2$O$_4$) crystal, cut and aligned to produce orthogonally polarized, collinearly propagating down-conversion photons at a center frequency of 702.2 nm. (There is of course nothing special about 702.2
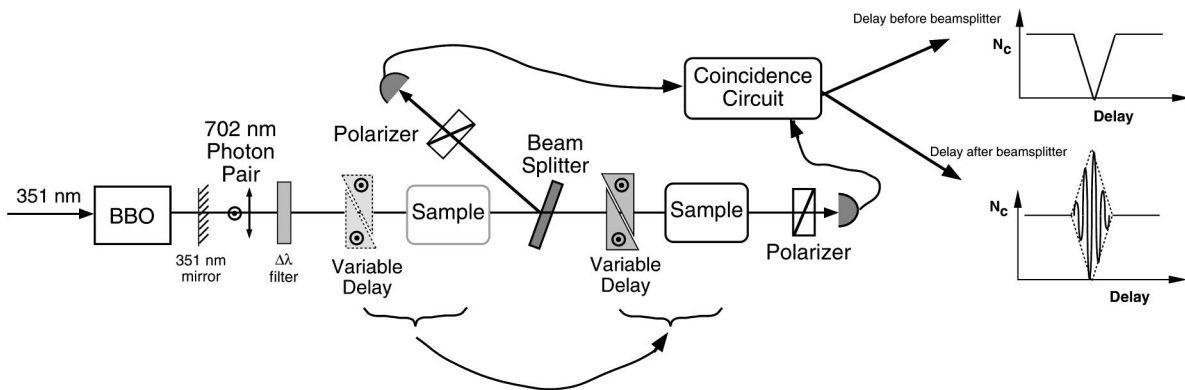

FIG. 4. PMD measurement scheme shown with two types of interference patterns. The lower (upper) pattern results when the variable delay is placed after (before) the beam splitter.

---

[2]We derive this result in Appendix A. The absence of the usual dispersion cancellation is also presented there.
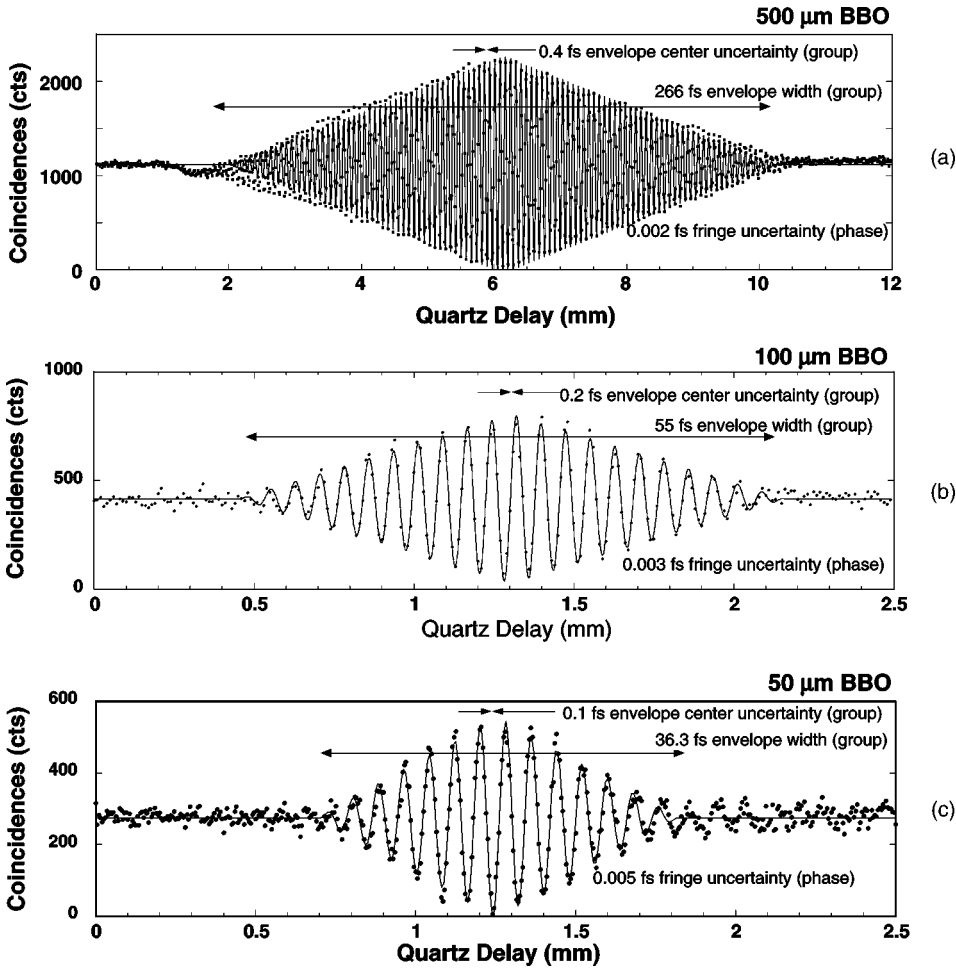
FIG. 5. Observed interference pattern for (a) 500-μm, (b) 50-μm, and (c) 50-μm BBO crystals. Data points are fit to a sine function with a triangular envelope indicated by the solid lines. The envelope widths and center uncertainties are given in terms of group delay, while the fringe uncertainty is given in terms of phase delay.

nm; other wavelengths can be measured by selecting other pump wavelengths.) A prism before the BBO crystal was used to reject laser light other than the 351.1-nm beam. A high efficiency, narrow bandwidth 351-nm mirror after the BBO crystal blocked the pump light from the rest of the system, while passing the longer wavelength downconverted light.

The differential optical delay line used in our setup is essentially a continuous variable-thickness birefringent plate. It consists of a pair of identical quartz wedges (with their optic axes oriented out of the page in the perspective of Fig. 4). One wedge is fixed, while the other can be translated along its hypotenuse to produce different amounts of delay without deviating the collinearly propagating beams. The differential group and phase delays produced by this variable-thickness quartz plate were calculated to be 32.192 and 29.981 fs/mm, respectively, at 702.2 nm as determined from published index-of-refraction data [15]. The delay line could be placed either in the common path (before the beam splitter) or in one arm after the beam splitter, providing postponed compensation as shown in the figure.

To prevent scattered pump light and ambient light from reaching the detectors, spectral filters of various widths centered at 702 nm were placed in the common path just before the beam splitter. The beam splitter was designed to have equal reflectance and transmittance, $|R|^2 = |T|^2 = 0.5$, with minimal polarization dependence. The polarizers in front of

each detector were oriented at $\theta_1 = \theta_2 = \pi/4$, to obtain counting rate profiles of the form (A31)—a triangular envelope filled with sinusoidal fringes. This polarization orientation allows photons of either polarization to be detected with equal probability.

We measured coincidence-counting rates as the delay thickness was varied. For an actual optical delay measurement, an unknown sample would also be inserted in the path, adjacent to the delay line wedges, and the shift in the interference pattern would then be observed. (Alternatively, the sample could remain in the beam path but be rotated 90°, producing twice the shift, as we shall see.) Our initial measurements, obtained without such a sample, are used simply to determine how well the interference features can be mapped and their positions located using the delay-line technique. This characterization is important in determining uncertainty limits of the method and it is crucial in choosing the optimum operating parameters (e.g., crystal length, measurement time, etc.) for making actual group- and phase-velocity measurements of a sample.

For the setup with the delay line before the beam splitter, we have previously found the triangle-shaped dip of Eq. (A33), with its width proportional to the BBO crystal length [6]. For the postponed delay configuration (the major focus of this paper), three lengths of BBO crystals (500, 100, and 50 μm) were tested. The data for the three crystal lengths are shown in Fig. 5. In each case, sinusoidal fringes are observed

TABLE I. Fit parameters and uncertainties for two measurements of the interference pattern.

Delay type	Fit result	BBO crystal length (μm)		
		500	100	50
Group	Envelope full width (W) (fs)	266.4	54.9	36.3
	Envelope center fit uncertainty ($\delta\mathcal{D}_{0e}$) (fs)	0.4	0.2	0.1
Phase	Fringe period (P) (fs)	2.358	2.305	2.387
	Fringe phase fit uncertainty ($\delta\mathcal{D}_{0f}$) (fs)	0.002	0.003	0.005

inside envelopes of finite width, and the peak fringe amplitude is nearly 100% of the constant rate outside of the envelope.

The spectral filters used for each of those measurements were broad[3] to avoid affecting the coherence of the down-converted light and thereby broadening the width of the interference envelopes. This was most successfully achieved for the 500-μm BBO measurement, where the triangular envelope shape is strikingly clear. The 50-μm BBO measurement exhibits some rounding of the triangular envelope [6]. In fact, it could be fit equally well with a Gaussian or triangular envelope, although triangular fit functions were used for each data set to simplify the comparison.

The fit function, a sine wave with a triangular envelope, was of the form

$$R_c = A\left\{1 + B\sin\left[2\pi\frac{(\mathcal{D}-\mathcal{D}_{0f})}{P}\right]\Lambda\left(\frac{\mathcal{D}-\mathcal{D}_{0e}}{\frac{1}{2}W}\right)\right\}, \quad (1)$$

where $\mathcal{D}$ is the length of post-delay quartz that is varied during a scan. This is the form of the coincidence rate predicted by Eq. (A32), with parameter A corresponding to a ''baseline'' pair detection rate and parameter B allowing for imperfect visibility of the sine modulation. The fringe phase and period are given by $\mathcal{D}_{0f}$ and P, respectively. According to Eq. (A32), the fringe period is given by

$$P = \frac{c}{\bar{\omega}[n_\mathcal{S}(\bar{\omega}) - n_\mathcal{F}(\bar{\omega})]}, \quad (2)$$

where $n_\mathcal{S}(\bar{\omega})$ and $n_\mathcal{F}(\bar{\omega})$ are the slow and fast indices of refraction in the post-delay material at the mean down-conversion frequency. The triangle function $\Lambda(x)$ is defined by Eq. (A27); the center of the triangular envelope is $\mathcal{D}_{0e}$, and W is its full width. Again according to Eq. (A32), we expect that the triangle full width should be given by

$$W = 2\tau_- \equiv 2\left(\left.\frac{dk_o}{d\omega}\right|_{\bar{\omega}} - \left.\frac{dk_e}{d\omega}\right|_{\bar{\omega}}\right)L, \quad (3)$$

that is, by twice the group delay walkoff over the full length L of the down-conversion crystal. The factor of 2 arises here because the delay is postponed until after the beam splitter, as discussed earlier.

The fitted values of P and W for our data are shown in Table I. The fitted values for the fringe period given in Table I agree with the expected value of 2.342 fs (half the pump laser period) to within 2%. The origin of the slight variations, as well as the small systematic deviations between fit and data seen in Fig. 5, are not presently understood and will be investigated further.

There is a possible ambiguity that must be considered when determining the phase delay. The group delay is uniquely determined by the shift of the interference envelope, but any observed shift in the phase of the fringes is consistent with an infinite number of possible phase delays (because additional delays of any whole number of fringes will produce the same apparent phase shift). Therefore, it would seem that we can only determine the phase delay up to an additive constant—an integer multiple of 2π. Fortunately, this ambiguity, which is common to all interferometric techniques for determining phase delay, can be dealt with in this case by noting the following relation between the group (n_g) and phase (n) indices of refraction:

$$n_g = n - \lambda\frac{dn}{d\lambda}. \quad (4)$$

Therefore, if a series of measurements of both n_g and n is made at different wavelengths, these quantities can be used to approximate $dn/d\lambda$. Then only one value of the aforementioned additive constant will provide consistency for both sets of measurements with Eq. (4).

Figure 6 shows an example of a shift due to a sample—a (0.902 ± 0.003)-mm quartz plate[4]—as it is rotated by 90°. Note that rotating the 0.902-mm sample is equivalent to inserting a 1.804-mm sample. For this particular measurement, the sample was actually located before the beam splitter, while the delay line was after the beam splitter. This allows us to clearly see the factor of 2 difference in the effects of delays before and after the beam splitter, predicted by Eq. (A31). In other words, after the beam splitter we should need twice the delay length—3.608 mm of quartz—to compensate

---

[3]The filters' spectral full widths at half maximum were 80 nm for the 500-μm crystal and 174 nm for the 100- and 50-μm crystals. The filters' spectral shapes were roughly between Gaussian and Lorentzian (see Ref. [6]).

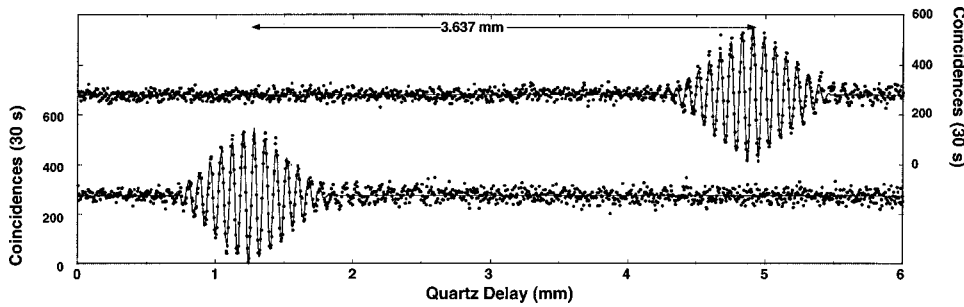[4]All uncertainties given in this paper refer to combined standard uncertainties, with coverage factor $k=1$.

FIG. 6. Displacement of an interference fringe envelope as a sample is rotated by 90°.

for the sample. The observed value was (3.637 ± 0.006) mm, which is equivalent to (0.909 ± 0.0015) mm of sample delay. This differs from the actual sample length by (0.007 ± 0.003) mm or about (0.2 ± 0.1) fs of sample delay. Note that this technique, as implemented, yields optical delays in terms of quartz length. Interpreting these delays as times depends on the prior knowledge of the dispersive properties of the quartz wedges and their geometry. Of course, a system using a conventional air delay line would eliminate this requirement.

Ultimately, the uncertainty with which group and phase delay can be determined depends on how well the envelope center and fringe phase of the interference feature can be located. To test the stability of the system, repeated scans of the interference shape were taken (without moving any sample). Figure 7 shows the resulting fit parameters for the envelope center and the fringe phase of those successive
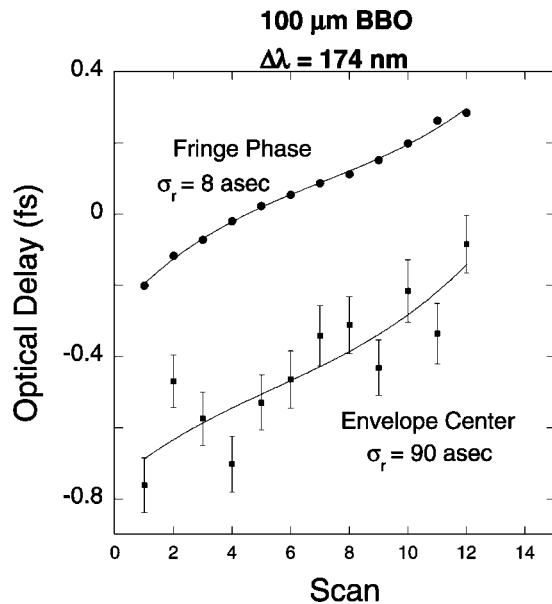

FIG. 7. Repeated scans of the two-photon interference feature were taken with a 100-μm BBO crystal and a 175-nm bandpass filter and fitted to Eq. (1). The parameters representing envelope center and the fringe phase are shown. The optical delay times were converted from quartz delay lengths using the appropriate quartz delay data (i.e., 29.981 fs/mm for the fringe phase and 32.192 fs/mm for the envelope center). These fit parameters were themselves fit to a low-order polynomial as indicated by the lines. The scatter (8 as and 90 as) from those lines indicates the repeatability and noise of each determination.

scans of the interference shape for the 100-μm BBO crystal. The error bars are the uncertainty of the fit determination. There is clearly an overall drift of the envelope center and the fringe phase with time of ~0.4 fs. We believe that this small shift, equivalent to ~0.1 μm, may be due to temperature variation of some birefringent component, as there was no attempt made at temperature stabilization. It is a significant point that because of the common path arrangement of this system, this low level of drift can be achieved without using any of the usual construction techniques required for interferometric stability. Looking beyond this relatively trivial drift, we have fit these two parameters to a low-order polynomial[5] to extract a true measure of the repeatability noise. This can be found from the rms deviation of the points from the smooth fit curve as seen in Fig. 7. This analysis yields a scatter of 90 as for the envelope center and 8 as for the fringe phase. Both of these values are consistent with the error bars, and the envelope uncertainty is consistent with our previous work with the original nonpostponed HOM setup [6]. These results show that with this postponed delay arrangement, phase delay can now be measured while retaining the capability and accuracy of the group-delay measurements.

In comparing this level of uncertainty for the differential group delay with that of most existing PMD techniques, we can see that this method offers the potential for significant improvement. A summary of five PMD measurement methods by Namihira and Maeda [16] lists accuracies ranging from 15 ps to 3 fs, while a more recent work claims an accuracy of 50 as [17]. In addition, a summary of dispersion measurements by Knox lists accuracies as good as ~0.1 fs [18].

DISCUSSION

We first note that in traditional HOM interferometers (without postponed compensation), the correlation envelope full widths expected for 500-, 100-, and 50-μm BBO crystals are 124, 24, and 12.4 fs, respectively [6], while we observe 266, 55, and 36 fs, respectively. We expect a factor of 2 increase in the observed dip widths because, as noted after Eq. (A31), a delay before the beam splitter requires a com-

_____

[5]The order of the polynomial was cut off at the point were no further significant reduction in the reduced χ^2 was obtained. For Fig. 7, this occurred for $n = 3$. This is essentially the point at which the uncertainties in the additional parameters exceed their values.

pensating delay of twice that after the beam splitter to achieve indistinguishability of the two types of coincidences and produce an interference. That the 50-μm measurement yields a factor significantly greater than 2 most likely results from some spectral limiting of the down-converted light by the spectral filter. While the 174-nm filter used is fairly broad, the slight rounding of the triangular envelope further indicates that some residual spectral limiting is occurring that is not due to the BBO crystal length alone, adding additional width to the observed shape [6,19].

It is also worth noting that the observed fringe phase uncertainties of 0.002–0.008 fs are extremely short times. They are, in fact, shorter than the constraint on the simultaneity of the creation of a down-converted photon pair. The uncertainty relation between time and energy gives a maximum time that can elapse between the creation of two photons of a pair. This time (Δt) between the creation of the two is limited by the uncertainty relation $\Delta E \Delta t \geq \hbar/2$, where ΔE is the energy deficit when one down-converted photon makes its appearance before its twin. This deficit would typically be about half the pump photon energy, so for $\lambda_p = 351$ nm, Δt is limited to ~ 0.2 fs. The fact that the fringe uncertainties are already much smaller than this value is not, however, a violation of the uncertainty principle. The uncertainty principle simply sets a limit on the minimum width of a distribution, not on how accurately its mean can be determined.

Finally, we note that in this experiment, both the central frequency and the full spectrum of the down-converted photons' wavepackets play a role. That is, even though the light is detected two photons at a time, each member of this ensemble registers as part of an interference pattern that manifests both single-frequency (phase-delay) and broadband (group-delay) properties. In some sense, each photon carries the full spectrum of the down-conversion, but, just like classical light, can exhibit features that depend either on the full spectrum or just on the central frequency.

In conclusion, we have demonstrated a two-photon interferometer that can be used to simultaneously measure group and phase delay with very high resolution and stability. The switch to a postponed compensation configuration maintains the resolution of the previous method, while adding phase-delay measurement capability. We have also provided (in Appendix A) a complete analysis of the effects of pre- and post-beam splitter delays, clearly showing that envelope shifts are due to group delay while fringe shifts are due to phase delay. There we also derive the unexpected result that GVD is not canceled in the postponed configuration, as it is in the traditional nonpostponed case.

It appears that, with the current system configuration with its inherent stability, resolutions of 0.002 fs are possible. As this is significantly below the time-energy uncertainty limit on the simultaneity of the creation of down-converted photon pairs, it will be interesting to see whether or how that limit can be seen to manifest itself in the interference line shape.

ACKNOWLEDGMENTS
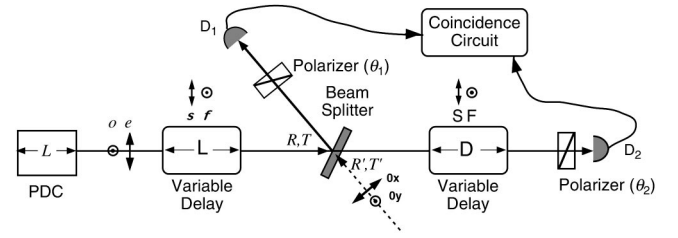
FIG. 8. Schematic of the collinear HOM interferometer with postponed compensation.

APPENDIX A: CALCULATION OF THE COINCIDENCE-COUNTING RATE

We consider the collinear version of the HOM interferometer, shown in Fig. 8, in which the signal and idler photons are orthogonally polarized along the extraordinary (e) and ordinary (o) axes of the PDC source and propagate in the same direction until reaching the beam splitter. Traditionally, delays between the two photons are imposed by placing various amounts of birefringent material before the beam splitter. Postponed compensation is introduced by means of additional birefringent material placed after the beam splitter. When the polarizers are oriented to transmit light polarized at 45° from the e or o axes, they destroy the distinguishing polarization information that would otherwise reveal which photon arrived at which detector. Because either photon may be transmitted through such a polarizer with equal probability, and because the polarization state of the photon after each polarizer cannot be used to reconstruct the original polarization state, the double-reflection and double-transmission processes are rendered indistinguishable, and therefore capable of interfering. The postponed compensation performs a similar function, by equalizing the relative arrival times of the photons and ensuring that no distinguishing information could be retrieved by making such a measurement.

The photon pair is generated by a cw-pumped type-II parametric downconverter (PDC) of length L. We assign the ''e'' polarization label to the signal photon, and the ''o'' label to the idler. The photons pass through a birefringent delay line of length $\mathcal{L}$, characterized by slow (s) and fast (f) indices of refraction (n_s, n_f), for the e and o polarizations, respectively. The photons then impinge onto a beam splitter (BS) with reflectivity R and transmissivity T. The reflected light passes through polarizer P_1, with its axis of transmission rotated clockwise by an angle θ_1 away from the ordinary polarization, and then impinges onto detector D_1. Meanwhile, the transmitted light passes through the postponed compensation delay line of length $\mathcal{D}$, characterized by slow (S) and fast (F) indices of refraction (n_S, n_F), and then through a similar polarizer P_2 oriented at angle θ_2 before reaching detector D_2.

We work in the interaction picture, with the state vector

evolving only according to the interaction Hamiltonian in the PDC medium, while the field operators evolve according to the free-space Hamiltonian and propagate from the PDC to the detectors. In this picture, the state vector for a pair of signal and idler photons emerging from the PDC is [20]

$$|\psi\rangle = M|\text{vac}\rangle + \eta|\psi^{(1)}\rangle, \tag{A1}$$

where η is a down-conversion efficiency parameter, M is a normalization constant, and

$$|\psi^{(1)}\rangle = \frac{\delta\omega}{2\pi} \sum_{\omega_s,\omega_i} \Phi(\omega_s,\omega_i)$$

$$\times \int_0^{T_i} dt' e^{-i(\omega_p-\omega_s-\omega_i)t'} |\omega_s\rangle_o |\omega_i\rangle_e. \tag{A2}$$

Here ω_p is the frequency of the monochromatic pump, while ω_s,ω_i are the signal and idler frequencies, and $\delta\omega$ is the spacing between frequency modes, to be taken to zero when calculations are performed. T_i is the interaction time, and the notation $|\omega\rangle_{o,e}$ refers to a single-photon Fock state in a mode of frequency ω and polarization o, e. The function

$$\Phi(\omega_s,\omega_i) = \text{sinc}\{[k_e(\omega_s)+k_o(\omega_s)-k_e(\omega_p)]L/2\} \tag{A3}$$

is the type-II collinear phase-matching function for the signal, idler, and pump beams in the PDC (with wave numbers k_e, k_o, and k_p, respectively).

Assuming the detectors are perfectly efficient, the probability that detector D_1 registers a photon within a time interval dt_1 centered at time t_1 and that detector D_2 registers a photon within dt_2 centered at t_2 is $p_{12}(t_1,t_2)dt_1dt_2$. The quantity p_{12} is an instantaneous probability density given by the normally ordered expectation value

$$p_{12}(t_1,t_2) = \langle\psi|:\hat{E}_1^{(-)}(t_1)\hat{E}_1^{(+)}(t_1)\hat{E}_2^{(-)}(t_2)\hat{E}_2^{(+)}(t_2):|\psi\rangle, \tag{A4}$$

where $\hat{E}_{1,2}$ are the operators for the electric fields reaching the detectors, dimensionalized so that the intensities $|\hat{E}_{1,2}|^2$ have units of photons per second. Each of these electric-field operators, in turn, may be written as a Fourier sum of independent, monochromatic field modes labeled at the PDC:

$$\hat{E}_1^{(+)}(t_1;\theta_1\mathcal{L}) = \left(\frac{\delta\omega}{2\pi}\right)^{1/2} \sum_\omega \left[\cos(\theta_1)\{R\hat{a}_e(\omega)e^{i[k_s(\omega)\mathcal{L}-\omega(t_1-\tau_1)]}+T'\hat{a}_{0x}(\omega)e^{-i\omega t_1}\}\right.$$

$$\left.+\sin(\theta_1)\{R\hat{a}_o(\omega)e^{i[k_f(\omega)\mathcal{L}-\omega(t_1-\tau_1)]}+T'\hat{a}_{0y}(\omega)e^{-i\omega t_1}\}\right] \tag{A5}$$

and

$$\hat{E}_2^{(+)}(t_2;\theta_2,\mathcal{L},\mathcal{D}) = \left(\frac{\delta\omega}{2\pi}\right)^{1/2} \sum_\omega \left[\cos(\theta_2)\{T\hat{a}_e(\omega)e^{i[k_s(\omega)\mathcal{L}+k_S(\omega)\mathcal{D}-\omega(t_2-r_2)]}+R'\hat{a}_{0x}(\omega)e^{-i\omega t_2}\}\right.$$

$$\left.+\sin(\theta_2)\{T\hat{a}_o(\omega)e^{i[k_f(\omega)\mathcal{L}+k_\mathcal{F}(\omega)\mathcal{D}-\omega(t_2-\tau_2)]}+R'\hat{a}_{0y}(\omega)e^{-i\omega t_2}\}\right]. \tag{A6}$$

In these expressions, $\tau_{1,2}$ are the times required for the light to propagate through all of the free-space portions of the paths from the PDC to detectors D_1 and D_2, respectively. Here $k_s(\omega)$ and $k_f(\omega)$ are the dispersion relations for the slow and fast polarizations within the first delay line, while $k_S(\omega)$ and $k_\mathcal{F}(\omega)$ are the dispersion relations within the postponed compensation delay line. Each electric-field operator also contains a vacuum component, $\hat{a}_{0x}$ or $\hat{a}_{0y}$, coupled in from the other side of the beam splitter via the reflectivity R' or transmissivity T', which will not contribute to the coincidence counting rate.

After inserting Eqs. (A2), (A5), and (A6) into Eq. (A4) and letting the annihilation operators act on the state vector, we have

$$P_{12}(t_1,t_2;\theta_1,\theta_2,\mathcal{L},\mathcal{D}) = \left| \frac{\eta}{(2\pi)^2} \int_0^\infty \int_0^\infty d\omega_s d\omega_i \Phi(\omega_s,\omega_i) \int_0^{T_i} dt' e^{i(\omega_p-\omega_s-\omega_i)} RT \right.$$

$$\times \left[\cos(\theta_1)\sin(\theta_2)e^{i\{[k_s(\omega_s)+k_f(\omega_i)]\mathcal{L}+k_\mathcal{F}(\omega_i)\mathcal{D}-\omega_s(t_1-\tau_1)-\omega_i(t_2-\tau_2)\}}\right.$$

$$\left.\left.+\sin(\theta_1)\cos(\theta_2)e^{i\{k_s(\omega_s)+k_f(\omega_i)]\mathcal{L}+k_S(\omega_s)\mathcal{D}-\omega_i(t_1-\tau_1)-\omega_s(t_2-\tau_2)\}}\right]\right|^2 \tag{A7}$$

in the limit as $\delta\omega \to 0$.

Because the interaction time is already much longer than the inverse bandwidth of the light allowed by the phase-matching function, we may extend the limits on the time integral to $\pm\infty$, so that this integral becomes $2\pi\delta(\omega_p-\omega_s-\omega_i)$. This can be used to eliminate one of the frequency integrals in Eq. (A7), so that

$$p_{12}(t_1,t_2;\theta_1,\theta_2,\mathcal{L},\mathcal{D}) = \left| \frac{\eta}{2\pi} \int_0^\infty d\omega_s \Phi(\omega_s,\omega_p-\omega_s) RT \right.$$

$$\times [\cos(\theta_1)\sin(\theta_2)e^{i\{[k_s(\omega_s)+k_e(\omega_p-\omega_s)]\mathcal{L}+k_{\mathcal{F}}(\omega_p-\omega_s)\mathcal{D}-\omega_s(t_1-\tau_1)-(\omega_p-\omega_s)(t_2-\tau_2)\}}$$

$$\left. + \sin(\theta_1)\cos(\theta_2)e^{i\{k_s(\omega_s)+k_e(\omega_p-\omega_s)]\mathcal{L}+k_{\mathcal{S}}(\omega_s)\mathcal{D}-(\omega_p-\omega_s)(t_1-\tau_1)-\omega_s(t_2-\tau_2)\}}] \right|^2. \tag{A8}$$

The total probability for a coincidence count, P_{12}, is the integral of $p_{12}(t_1,t_2)$ over all possible photon arrival times t_1,t_2 within the coincidence resolving time. However, most of this joint detection probability will accumulate over a much smaller range of arrival times, namely, the mutual coherence time of the two-photon wave packet. Therefore, we can extend the limits of the time integrations to $\pm\infty$, so that

$$P_{12}(\theta_1,\theta_2,\mathcal{L},\mathcal{D}) = \int_{-\infty}^\infty \int_{-\infty}^\infty dt_1 dt_2 p_{12}(t_1,t_2;\theta_1,\theta_2,\mathcal{L},\mathcal{D}). \tag{A9}$$

Inserting Eq. (A8) into Eq. (A9), we obtain, after taking advantage of the Dirac δ functions in frequency produced by the time integrations,

$$P_{12}(\theta_1,\theta_2,\mathcal{L},\mathcal{D}) = |\eta|^2 \frac{|RT|^2}{2} \{[1-\cos(2\theta_1)\cos(2\theta_2)]B + \sin(2\theta_1)\sin(2\theta_2)[F(\mathcal{L},\mathcal{D})+G(\mathcal{L},\mathcal{D})]\}, \tag{A10}$$

where

$$B \equiv \int_0^\infty d\omega_s |\Phi(\omega_s,\omega_p-\omega_s)|^2, \tag{A11}$$

$$F(\mathcal{L},\mathcal{D}) \equiv \int_0^\infty d\omega_s \Phi(\omega_s,\omega_p-\omega_s)\Phi^*(\omega_p-\omega_s,\omega_s)e^{i\{[k_s(\omega_s)-k_s(\omega_p-\omega_s)+k_e(\omega_p-\omega_s)-k_e(\omega_s)]\mathcal{L}+[k_{\mathcal{S}}(\omega_s)-k_{\mathcal{F}}(\omega_s)]\mathcal{D}\}}, \tag{A12}$$

and

$$G(\mathcal{L},\mathcal{D}) \equiv \int_0^\infty d\omega_s \Phi(\omega_s,\omega_p-\omega_s)\Phi^*(\omega_p-\omega_s,\omega_s)e^{i\{k_s(\omega_s)-k_s(\omega_p-\omega_s)+k_e(\omega_p-\omega_s)-k_e(\omega_s)]\mathcal{L}+[k_{\mathcal{S}}(\omega_p-\omega_s)-k_{\mathcal{F}}(\omega_p-\omega_s)]\mathcal{D}\}}. \tag{A13}$$

The integrals in Eqs. (A11)–(A13) may be performed with the help of a Taylor series expansion of the arguments of Φ about the mean (or degenerate) down-conversion frequency, $\bar{\omega}$. The pump frequency is fixed at $2\bar{\omega}$. To first order in frequency, this produces

$$\Phi(\omega_s,\omega_p-\omega_s) \cong \text{sinc}(\tfrac{1}{2}\tau_-\nu_s), \tag{A14}$$

where

$$\nu_s \equiv (\omega_s-\bar{\omega}) \tag{A15}$$

and

$$\tau_- \equiv \left(\left. \frac{dk_o}{d\omega} \right|_{\bar{\omega}} - \left. \frac{dk_e}{d\omega} \right|_{\bar{\omega}} \right) L \tag{A16}$$

is the "group delay walkoff," or difference in group-delay times for light traveling the length of the PDC medium with ordinary or extraordinary polarization. We substitute Eq. (A14) into Eq. (A11) and integrate to find

$$B \cong \int_{-\infty}^\infty d\nu_s \, \text{sinc}^2(\tfrac{1}{2}\tau_-\nu_s)$$

$$= \frac{2\pi}{\tau_-}. \tag{A17}$$

In the same fashion, Eq. (A12) may also be written as

$$F(\mathcal{L},\mathcal{D}) \equiv \int_{-\infty}^{\infty} d\nu_s \, \mathrm{sinc}^2(\tfrac{1}{2}\,\tau_-\nu_s) e^{i\{[k_\searrow(\bar{\omega}+\nu_s)-k_\searrow(\bar{\omega}-\nu_s)+k_\nearrow(\bar{\omega}-\nu_s)-k_\nearrow(\bar{\omega}+\nu_s)]\mathcal{L}+[k_\mathcal{S}(\bar{\omega}+\nu_s)-k_{\mathcal{FS}}(\bar{\omega}+\nu_s)]\mathcal{D}\}}. \tag{A18}$$

To perform this integration, we will make two more Taylor series expansions. First we expand the coefficients of $\mathcal{L}$, the terms corresponding to propagation through the first delay line:

$$[k_\searrow(\bar{\omega}+\nu_s)-k_\searrow(\bar{\omega}-\nu_s)+k_\nearrow(\bar{\omega}-\nu_s)-k_\nearrow(\bar{\omega}+\nu_s)]\mathcal{L}$$

$$= \left[k_\searrow|_{\bar{\omega}}-k_\searrow|_{\bar{\omega}}+k_\nearrow|_{\bar{\omega}}-k_\nearrow|_{\bar{\omega}}+\nu_s\frac{dk_\searrow}{d\omega}\bigg|_{\bar{\omega}}+\nu_s\frac{dk_\searrow}{d\omega}\bigg|_{\bar{\omega}}-\nu_s\frac{dk_\nearrow}{d\omega}\bigg|_{\bar{\omega}}-\nu_s\frac{dk_\nearrow}{d\omega}\bigg|_{\bar{\omega}} \right.$$

$$\left. +\tfrac{1}{2}\,\nu_s^2\frac{d^2k_\searrow}{d\omega^2}\bigg|_{\bar{\omega}}-\tfrac{1}{2}\,\nu_s^2\frac{d^2k_\searrow}{d\omega^2}\bigg|_{\bar{\omega}}+\tfrac{1}{2}\,\nu_s^2\frac{d^2k_\nearrow}{d\omega^2}\bigg|_{\bar{\omega}}-\tfrac{1}{2}\,\nu_s^2\frac{d^2k_\nearrow}{d\omega^2}\bigg|_{\bar{\omega}}+\cdots \right]\mathcal{L}. \tag{A19}$$

The first four terms, involving phase-velocity differences in the birefringent material, cancel completely. The last four terms, involving group-velocity dispersion (GVD), also cancel each other completely—this is the dispersion cancellation effect discovered by Steinberg *et al.* Like the phase-velocity cancellation, it occurs because the frequencies of the two photons are entangled so that if one has frequency $\bar{\omega}+\nu_s$, the other must have frequency $\bar{\omega}-\nu_s$. We can see from the form of Eq. (A19) that all subsequent terms carrying an even power of ν_s will be similarly canceled, leaving only the terms with odd powers of ν_s. The lowest-order surviving terms may be rewritten to give

$$[k_\searrow(\bar{\omega}+\nu_s)-k_\searrow(\bar{\omega}-\nu_s)+k_\nearrow(\bar{\omega}-\nu_s)-k_\nearrow(\bar{\omega}+\nu_s)]\mathcal{L}$$
$$\cong 2\nu_s\tau_\nearrow(\mathcal{L}), \tag{A20}$$

where

$$\tau_\nearrow(\mathcal{L}) \equiv \left[\frac{dk_\searrow}{d\omega}\bigg|_{\bar{\omega}}-\frac{dk_\nearrow}{d\omega}\bigg|_{\bar{\omega}} \right]\mathcal{L} \tag{A21}$$

is the group-delay walkoff in the delay line.

Now the terms in Eq. (A18) corresponding to propagation through the postponed compensation delay line can be similarly expanded, and it is at this point that the differences between predelay (before the beam splitter) and postdelay (after the beam splitter) become apparent. The relative phase accumulated in the postdelay is

$$[k_\mathcal{S}(\bar{\omega}+\nu_s)-K_\mathcal{F}(\bar{\omega}+\nu_s)]\mathcal{D}$$

$$= \left[k_\mathcal{S}|_{\bar{\omega}}-k_\mathcal{F}|_{\bar{\omega}}+\nu_s\frac{dk_\mathcal{S}}{d\omega}\bigg|_{\bar{\omega}}-\nu_s\frac{dk_\mathcal{F}}{d\omega}\bigg|_{\bar{\omega}} \right.$$

$$\left. +\tfrac{1}{2}\,\nu_s^2\frac{d^2k_\mathcal{S}}{d\omega^2}\bigg|_{\bar{\omega}}-\tfrac{1}{2}\,\nu_s^2\frac{d^2k_\mathcal{F}}{d\omega^2}\bigg|_{\bar{\omega}}+\cdots \right]\mathcal{D}. \tag{A22}$$

Note that no cancellations of any kind occur here, except in the case of balanced dispersion [11]. In particular, the GVD is not canceled for the light which travels through the postponed delay line. For what follows, we will choose to ignore the GVD terms, and retain only the constant and first-order terms in the expansion, so that

$$[k_\mathcal{S}(\bar{\omega}+\nu_s)-k_\mathcal{F}(\bar{\omega}+\nu_s)]\mathcal{D} \cong \bar{\omega}[n_\mathcal{S}(\bar{\omega})-n_\mathcal{F}(\bar{\omega})]\frac{\mathcal{D}}{c}$$
$$+\nu_s\tau_{\mathcal{SF}}(\mathcal{D}), \tag{A23}$$

where

$$\tau_{\mathcal{SF}}(\mathcal{D}) \equiv \left[\frac{dk_\mathcal{S}}{d\omega}\bigg|_{\bar{\omega}}-\frac{dk_\mathcal{F}}{d\omega}\bigg|_{\bar{\omega}} \right]\mathcal{D} \tag{A24}$$

is the group-delay walkoff in the postponed delay line.

With the approximations of Eqs. (A20) and (A23) in place, we may now rewrite Eq. (A18) as

$$F(\mathcal{L},\mathcal{D}) = e^{i\bar{\omega}[n_\mathcal{S}(\bar{\omega})-n_\mathcal{F}(\bar{\omega})](\mathcal{D}/c)}\int_{-\infty}^{\infty} d\nu_s$$

$$\times \mathrm{sinc}^2(\tfrac{1}{2}\,\tau_-\nu_s)e^{i\nu_s[2\tau_\nearrow(\mathcal{L})+\tau_{\mathcal{SF}}(\mathcal{D})]}. \tag{A25}$$

The integral is an inverse Fourier transform which yields

$$F(\mathcal{L},\mathcal{D}) = \left(\frac{2\pi}{\tau_-}\right)e^{i\bar{\omega}[n_\mathcal{S}(\bar{\omega})-n_\mathcal{F}(\bar{\omega})](\mathcal{D}/c)}\Lambda\left(\frac{\tau_\nearrow(\mathcal{L})+\tfrac{1}{2}\,\tau_{\mathcal{SF}}(\mathcal{D})}{\tfrac{1}{2}\,\tau_-}\right) \tag{A26}$$

where the triangle function is defined as

$$\Lambda(x) = \begin{cases} 1-|x|, & -1\leqslant x\leqslant 1 \\ 0 & \text{otherwise.} \end{cases} \tag{A27}$$

In a similar fashion, Eq. (A13) may be evaluated to give

$$G(\mathcal{L},\mathcal{D})$$

$$= \left(\frac{2\pi}{\tau_-}\right)e^{-i\bar{\omega}[n_\mathcal{S}(\bar{\omega})-n_\mathcal{F}(\bar{\omega})](\mathcal{D}/c)}\Lambda\left(\frac{\tau_\nearrow(\mathcal{L})+\tfrac{1}{2}\,\tau_{\mathcal{SF}}(\mathcal{D})}{\tfrac{1}{2}\,\tau_-}\right) \tag{A28}$$
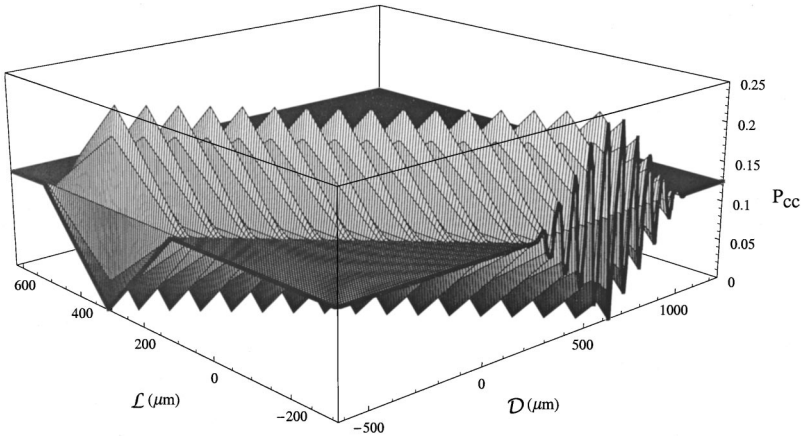
$$= F^*(\mathcal{L},\mathcal{D}).$$

FIG. 9. Probability of obtaining a coincidence count (P_{cc}), given that a photon pair has been emitted, as a function of the lengths of quartz delay lines placed before ($\mathcal{L}$) and after ($\mathcal{D}$) the beam splitter.

Inserting Eqs. (A28), (A26), and (A17) into Eq. (A10), we have, for the total probability of a coincidence count,

$$P_{12}(\theta_1,\theta_2,\mathcal{L},\mathcal{D}) = P_E \frac{|RT|^2}{2}\left\{ 1-\cos(2\theta_1)\cos(2\theta_2)\right.$$

$$+\sin(2\theta_1)\sin(2\theta_2)\cos\left(\bar{\omega}[n_{\mathcal{S}}(\bar{\omega})\right.$$

$$\left.\left.-n_{\mathcal{F}}(\bar{\omega})]\frac{\mathcal{D}}{c}\right)\Lambda\left(\frac{\tau_{\mathcal{S}}(\mathcal{L})+\frac{1}{2}\tau_{\mathcal{SF}}(\mathcal{D})}{\frac{1}{2}\tau_-}\right)\right\},$$

$$(A29)$$

where

$$P_E \equiv |\eta|^2 \langle\psi^{(1)}|\psi^{(1)}\rangle$$

$$= |\eta|^2\left(\frac{2\pi}{\tau_-}\right) \qquad (A30)$$

is the probability that a signal and idler photon pair is emitted by the PDC within the interaction time. If the beam splitter is chosen to have $|R|=|T|=0.5$, and the polarizer settings are chosen for maximum dip visibility, $\theta_1=\theta_2=\pi/4$, then the probability of a coincidence count given that a photon pair is generated is

$$\mathcal{P}_{12}(\pi/4,\pi/4,\mathcal{L},\mathcal{D})$$

$$\equiv \frac{P_{12}(\pi/4,\pi/4,\mathcal{L},\mathcal{D})}{P_E}$$

$$= \frac{1}{8}\left\{1-\cos\left(\bar{\omega}[n_{\mathcal{S}}(\bar{\omega}-n_{\mathcal{F}}(\bar{\omega})]\frac{\mathcal{D}}{c}\right)\right.$$

$$\left.\times\Lambda\left(\frac{\tau_{\mathcal{S}}(\mathcal{L})+\frac{1}{2}\tau_{\mathcal{SF}}(\mathcal{D})}{\frac{1}{2}\tau_-}\right)\right\}. \qquad (A31)$$

This quantity is plotted in Fig. 9. As the length of predelay material, $\mathcal{L}$, is changed while the postdelay, $\mathcal{D}$, is kept fixed, the coincidence-counting rate traces out a familiar triangle-shaped dip [5]. The value of the counting rate within this dip

is determined by the group-delay walkoff in the delay line, $\tau_{\mathcal{S}}(\mathcal{L})$, as compared with the group-delay walkoff in the PDC, τ_-. On the other hand, as the length of postponed delay $\mathcal{D}$ is changed, two effects are at work: the triangular envelope is still traced out according to the group-delay walkoff, $\tau_{\mathcal{S}}(\mathcal{D})$, but this envelope is modulated by a sinusoidal fringe pattern that oscillates according to the relative phase delays for the two polarizations in the medium. Also, as noted previously, the amount of postponed group delay required to scan through the dip is exactly double the amount required if it is placed before the beam splitter [8,14].

If the interferometer contains only postponed delay, $\mathcal{D}$, but no delays before the beam splitter, then as $\mathcal{D}$ is scanned we will observe the cross section of this figure that displays the fringes: Eq. (A31) becomes

$$\mathcal{P}_{12}(\pi/4,\pi/4,\mathcal{D}) = \frac{1}{8}\left\{1-\cos\left(\bar{\omega}[n_{\mathcal{S}}(\bar{\omega})\right.\right.$$

$$\left.\left.-n_{\mathcal{F}}(\bar{\omega})]\frac{\mathcal{D}}{c}\right)\Lambda\left(\frac{\tau_{\mathcal{SF}}(\mathcal{D})}{\tau_-}\right)\right\}.$$

$$(A32)$$

Note that the half-width of the triangle function, in the denominator of the argument of Λ, is now τ_- and not $\tau_-/2$.

On the other hand, in the absence of any postponed compensation, Eq. (A31) reduces to

$$\mathcal{P}_{12}(\pi/4,\pi/4,\mathcal{L},0) = \frac{1}{8}\left\{1-\Lambda\left(\frac{\tau_{\mathcal{S}}(\mathcal{L})}{\frac{1}{2}\tau_-}\right)\right\}, \qquad (A33)$$

and we recover the usual triangle-shaped dip for type-II cw-pumped HOM interference [5]. In this expression, only the group delays appear. However, at least one report seems to claim, erroneously, that the phase delays, and not the group delays, govern the shape of the dip [21]. Therefore, we must emphasize that for delays occurring before the beam splitter, it is only the group delay that matters when tracing out the HOM coincidence dip. This is what one would expect based on classical intuition, and based on the demonstration by Steinberg *et al.* [9] that identified the propagation velocity of single-photon wave packets in media as the group velocity.

[1] L. Mandel, in *More Things in Heaven and Earth: A Celebration of Physics at the Millennium*, edited by B. Bederson (Springer-Verlag, New York, 1999), p. 460.

[2] A. Zeilinger, in *More Things in Heaven and Earth: A Celebration of Physics at the Millennium* (Ref. [1]), p. 482.

[3] A. Zeilinger, Phys. World **11** (3), 35 (1998).

[4] A. Migdall, Phys. Today **52** (1), 41 (1999).

[5] A. V. Sergienko, Y. H. Shih, and M. H. Rubin, J. Opt. Soc. Am. B **12**, 859 (1995).

[6] E. Dauler *et al.*, J. Res. Natl. Inst. Stand. Technol. **104**, 1 (1999).

[7] C. K. Hong, Z. Y. Ou, and L. Mandel, Phys. Rev. Lett. **59**, 2044 (1987).

[8] T. B. Pittman *et al.*, Phys. Rev. Lett. **77**, 1917 (1996).

[9] A. M. Steinberg, P. G. Kwiat, and R. Y. Chiao, Phys. Rev. Lett. **68**, 2421 (1992).

[10] A. M. Steinberg, P. G. Kwiat, and R. Y. Chiao, Phys. Rev. A **45**, 6659 (1992).

[11] T. S. Larchuk, M. C. Teich, and B. E. A. Saleh, Phys. Rev. A **52**, 4145 (1995).

[12] R. Ghosh, C. K. Hong, Z. Y. Ou, and L. Mandel, Phys. Rev. A **34**, 3962 (1986).

[13] A. M. Steinberg, P. G. Kwiat, and R. Y. Chiao, Phys. Rev. Lett. **71**, 708 (1993).

[14] T. B. Pittman, Ph.D. thesis, University of Maryland, Baltimore County (UMBC), 1996 (unpublished).

[15] E. D. Palik, *Handbook of Optical Constants of Solids* (Academic, Orlando, 1985).

[16] Y. Nimihira and J. Maeda, Electron. Lett. **28**, 2265 (1992).

[17] B. L. Heffner, Opt. Lett. **18**, 2102 (1993).

[18] W. H. Knox, Appl. Phys. B: Lasers Opt. **58**, 225 (1994).

[19] N. Boeuf *et al.*, Opt. Eng. **39**, 1016 (2000).

[20] L. Mandel and E. Wolf, *Optical Coherence and Quantum Optics* (Cambridge University Press, Cambridge, 1995).

[21] M. H. Rubin, D. N. Klyshko, Y. H. Shih, and A. V. Sergienko, Phys. Rev. A **50**, 5122 (1994).